A three-dimensional model of single-electron tunneling between a conductive probe and a localized electronic state in a dielectric

N. Zheng, C. C. Williams,[a] E. G. Mishchenko, and E. Bussmann[b]
Department of Physics, University of Utah, 115 S 1400E, Room 201, Salt Lake City, Utah 84112

(Received 28 June 2006; accepted 12 January 2007; published online 1 May 2007)

Motivated by recent measurements of force detected single-electron tunneling, we present a three-dimensional model for the tunneling rate between a metallic tip and a localized electronic state in a dielectric surface. The tip is assumed to be semi-infinite, with electron wave functions approximated by plane waves. A localized electron state in the dielectric sample is approximated by a spherical quantum well. The tunneling rate is obtained with the help of Bardeen's approach and is compared with the results for a one-dimensional square barrier model. A comparison with experimental data is also presented. © *2007 American Institute of Physics*.
[DOI: 10.1063/1.2710438]

I. INTRODUCTION

Scanning tunneling microscopy[1] (STM) is very useful for characterizing electron states of metallic and semiconducting samples with atomic resolution. However, limitations due to the minimum detectable current prevent STM from being used with nonconducting samples. A single-electron tunneling force method has been developed to characterize localized, electrically isolated states in insulating materials.[2–5]

Previously, a one-dimensional square barrier model[6] has been used to estimate the tunneling rate for a metal-vacuum-localized state system. Such a calculation can provide a reasonable estimate of the tunneling rate and the depth of localized states. However, one-dimensional models ignore complications due to the three-dimensional character of the wave functions in the tip and dielectric sample. The oversimplification restricts the accuracy of results.

In the present paper a three-dimensional model is presented for computation of the electron tunneling rate between a metallic tip and a localized electronic state in a dielectric sample. Since the size of the tip is typically much larger than the radius of the localized state, the tip is assumed semi-infinite. Electron wave functions in the metallic tip are approximated with plane waves. The wave function of the localized state, typically a point defect, is approximated with a spherical potential well.

It is convenient to utilize the Bardeen approach,[7–10] which gives the elastic tunneling rate $W_{\mu\nu}$ from a state ψ_μ with energy E_μ to another single state ψ_ν with energy E_ν,

$$W_{\mu\nu} = \frac{2\pi}{\hbar}|M_{\mu\nu}|^2 \delta(E_\mu - E_\nu), \tag{1}$$

where $M_{\mu\nu}$ is the tunneling matrix element determined by the surface integral taken over a surface S between the tip and the localized state,

$$M_{\mu\nu} = -\frac{\hbar^2}{2m}\int_S (\psi_\nu^* \nabla \psi_\mu - \psi_\mu \nabla \psi_\nu^*)\cdot d\mathbf{s}. \tag{2}$$

Conservation of the tunneling probability current ensures that the particular choice of the surface S does not affect the tunneling matrix element $M_{\mu\nu}$. The total rate of tunneling into a localized state is given by a sum over all electron states in the metallic tip. The number of states within the elementary interval of phase space (for both spin directions) is $\Delta n = (V/4\pi^3)k^2 \sin\theta dk d\theta d\varphi$, where V is the tip volume. Here we utilize spherical coordinates with the angle θ between the direction of electron propagation and the direction normal to the surface and φ the azimuthal angle about the normal direction. It is convenient to take the surface of the dielectric as the integration surface. Assuming that the localized state is empty, we obtain for the total tunneling rate,

$$W = \frac{V}{\pi\hbar}\int_{-\infty}^{+\infty} \delta[E_k(k) - E_0]k^2 f(E_k)dk \int_0^\pi |M(k,\theta)|^2 \sin\theta d\theta, \tag{3}$$

$$M(k,\theta) = -\frac{\hbar^2}{2}\left(\int_{z=-h+0} \frac{1}{m^*}\psi_T^* \frac{\partial \psi_S}{\partial z} ds - \int_{z=-h-0} \frac{1}{m}\psi_S \frac{\partial \psi_T^*}{\partial z} ds\right), \tag{4}$$

where m and m^* are the vacuum electron mass and the effective mass in the conduction band of the dielectric, respectively, $f(E_k)$ is Fermi function, $z=-h$ is the surface of the dielectric, and $E_k(k)=\hbar^2k^2/2m$ is the energy of the electron state in the metallic tip to/from which the electron tunnels. This state has a wave vector magnitude k measured relative to the bottom of the energy band in the metal tip. E_0 is the energy of the localized state, ψ_T is the wave function of the electron tip state at the dielectric surface, and ψ_S is the wave function of the localized state at the dielectric surface. Figures 1(a) and 1(b) show the tunneling measurement geometry and the band structure of the tip-insulator system.

[a]Author to whom correspondence should be addressed; electronic mail: clayton@physics.utah.edu
[b]Present address: Sandia National Laboratories, Albuquerque, NM 87185.

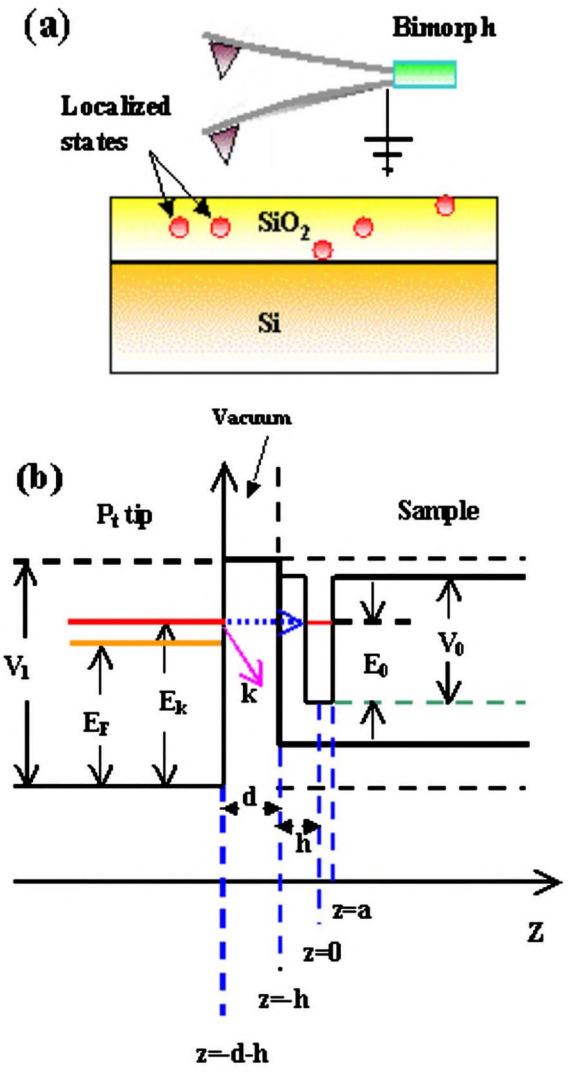

FIG. 1. (Color online) (a) A schematic diagram of the tip-sample system for single-electron tunneling. Tunneling is not observed under typical conditions for a tip-sample gap >2.0 nm. (b) The energy band structure and space coordinate of the tip-sample system for single-electron tunneling.

II. ELECTRONIC WAVE FUNCTIONS IN THE TIP AND THE DIELECTRIC SAMPLE

The electron wave functions in the tip are approximated with plane waves. The normalized tip wave functions in the vacuum can be written as[11]

$$\psi_T = \frac{1}{\sqrt{2V}} \frac{2ik_z}{ik_z - k_z'} \exp(ik_x x + ik_y y)\exp[-k_z'(z+d+h)], \tag{5}$$

where $k_z' = \sqrt{2mV_1/\hbar^2 - k_z^2}$, and V_1 is the height of the vacuum barrier relative to the bottom of energy band in the metallic tip [see Fig. 1(b)]. Note that the origin of the z coordinate is found at the center of the localized state, and the tip surface is found at $z=-d-h$. Also note that the tip wave functions in the gap do not include any terms due to the boundary condition associated with the surface of the dielectric. This approximation is valid when the wave functions from the tip have small values at the dielectric surface, $e^{-k_z' d} \ll 1$.

The localized state in the dielectric sample is approximated with the help of a spherical quantum well,

$$V(r) = \begin{cases} 0, & r < a \\ V_0, & r > a, \end{cases} \tag{6}$$

where V_0 is the depth of the localized electronic state with respect to the conduction band edge and a is the radius of the finite spherical quantum well. The center of the well is located at a distance h from the dielectric surface, see Fig. 1(b). Assuming that tunneling occurs into (or from) the ground state, the normalized electron wave function for $r > a$ can be written as[6]

$$\psi_S(r) = \frac{B}{\sqrt{4\pi}} * \frac{e^{-q'r}}{r},$$

$$B = \frac{e^{q'a}\sin(qa)}{[a/2 - \sin(2qa)/4q + \sin^2(2qa)/2q']^{1/2}}, \tag{7}$$

where $q = \sqrt{2m^* E_0}/\hbar$, $q' = \sqrt{2m^*(V_0 - E_0)}/\hbar$, and m^* is the effective mass in the dielectric conduction band. The energy E_0 is determined by the equation, $q\cot(qa) = -q'$.

Here, the wave function of the localized electronic state in the dielectric does not include additional terms required by the boundary conditions of the dielectric surface. This approximation is reasonable when the value of the wave function at the dielectric surface is small, that is, $e^{-q'h} \ll 1$.

III. CALCULATION OF THE TUNNELING RATE *W* AND DISCUSSION OF THE THREE-DIMENSIONAL MODEL

As shown in Fig. 1(b), we have chosen $z=0$ to correspond to the center of spherical quantum well and the plane $z=-h$ as the surface of the dielectric, where the tunneling matrix element is calculated by Eq. (4). Substituting electron wave functions into this expression we obtain for the matrix element,

$$M(k,\theta) = 2\pi C e^{-k_z' d} \int_0^{+\infty} f(\rho,\theta) J_0(\rho k \sin\theta)\rho d\rho, \tag{8}$$

where $J_0(\rho k \sin\theta)$ is the zeroth order Bessel function.

Here we introduced the following notation:

$$f(\rho,\theta) = e^{-q' r(\rho)}\left[\frac{m}{m^*}\frac{z}{r(\rho)^3} + \frac{m}{m^*}\frac{zq'}{r(\rho)^2} - \frac{k_z'(\theta)}{r(\rho)}\right],$$

$$C = \frac{T^* B\hbar^2}{4m\sqrt{2\pi V}},$$

$$T = \frac{2ik_z}{ik_z - k_z'}, \quad T^* = \frac{2ik_z}{ik_z + k_z'}, \quad k_z' = \sqrt{\frac{2mV_1}{\hbar^2} - k_z^2}, \tag{9}$$

$$k = \sqrt{\frac{2mE_k}{\hbar^2}},$$

and utilized polar coordinates in the plane of integration, $r = \sqrt{\rho^2 + z^2}$. Substituting the matrix element (8) into Eq. (3),

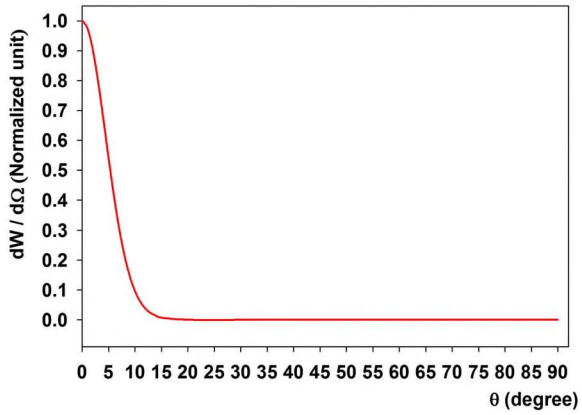

FIG. 2. (Color online) Illustration of the relation between tunneling rate (normalized unit) per solid angle and angle θ.

we first integrate over the absolute value of the electron momentum k, eliminating the delta function,

$$W = \frac{\hbar}{4mk}\int_0^{\pi} F(\theta)\sin\theta d\theta,$$

$$F(\theta) = |T|^2 B^2 e^{-2k_z' d}\left|\int_0^{+\infty} f(\rho,\theta)J_0(\rho k\sin\theta)\rho d\rho\right|^2 f(E_k)k^2. \tag{10}$$

Here k is determined from the equation $E_k(k)=E_0$. The integration can be performed numerically. For an analytical estimate of the tunneling rate, we note that $F(\theta)$ has a sharp Gaussian dependence on the angle (see Fig. 2). This is the result of the rapid decay of the wave functions normal to the dielectric surface at high angles. In Fig. 2, the following tip-sample parameters were used. The work function of the platinum tip is $(V_1-E_f=5.7$ eV), the band gap of the SiO_2 sample is 8.8 eV, and the offset between vacuum level and conduction band of SiO_2 is 0.9 eV. The tip-sample gap d is 1 nm, state depth h is 1.25 nm, and height V_0 of spherical quantum well formed by the localized state is 4.5 eV. The radius a of quantum well is 0.25 nm, and the effective mass m^* in the SiO_2 is 0.3 times that of a free electron. Calculating the Gaussian integral we obtain

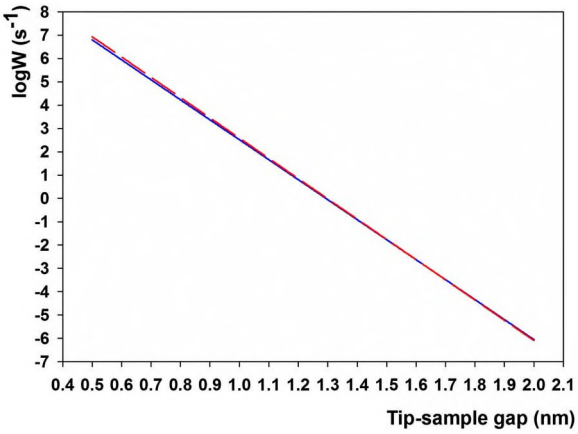

FIG. 3. (Color online) Comparison of tunneling rate between numerical calculation and analytical approximation. The blue solid line is from the analytical approximation, and the red dashed line is from the exact numerical integration. In the simulation, all parameters are the same as those in Fig. 2.

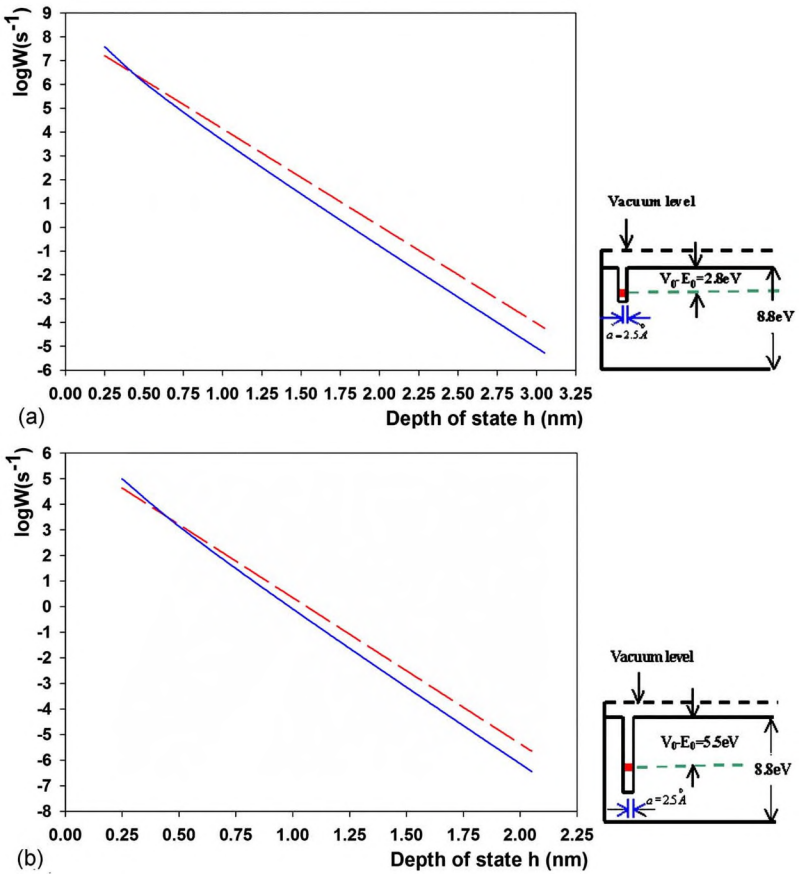

FIG. 4. (Color online) (a) Simulation curve of tunneling rate vs localized state depth and comparison of tunneling rate curve between the 3D analytical model (solid blue) and the 1D model (dashed red). All parameters in this simulation are the same as those in Fig. 2. except for V_0 and h. (b) Simulation curve of tunneling rate vs localized state depth and comparison of tunneling rate curve between the 3D analytical model (solid blue) and the 1D model (dashed red). All parameters in this simulation are the same as those in Fig. 2. except for V_0 and h.

$$W_{3D} = \frac{\hbar^2 B^2 E_k^{1/2}}{2\sqrt{2}m^{3/2}V_1} e^{-2d\sqrt{2m(V_1-E_k)/\hbar^2}} \left[\frac{m}{m^*} + \frac{m}{m^*} hq' + h\sqrt{\frac{2m(V_1-E_k)}{\hbar^2}} \right]^2 \frac{e^{-2q'h}}{q'h^3}. \quad (11)$$

A comparison of the exact numerical integration of Eq. (10) and the approximate analytical result [Eq. (11)] is seen in Fig. 3. The difference between the two is below 25% for typical experimental conditions. Note that this equation is approximately valid when the wave functions from the tip and state in the dielectric have small values at the dielectric surface.

It is instructive to compare the analytical tunneling rate with the predictions of the one-dimensional model. In the latter, the localized state is approximated by a one-dimensional rectangular potential. Using Bardeen's approach, a simple calculation yields

$$W_{1D} = \frac{\sqrt{2}\hbar^2 B^2 E_k^{1/2}}{m^{3/2}V_1} \left(\frac{m}{m^*} q' + k' \right)^2 e^{-2d\sqrt{2m(V_1-E_k)/\hbar^2}} e^{-2q'h}, \quad (12)$$

$$k' = \sqrt{\frac{2m(V_1-E_k)}{\hbar^2}}.$$

Comparison of Eq. (12) with the analytical three-dimensional result demonstrates that the one-dimensional model overestimates the tunneling rate, $W_{1D} > W_{3D}$, except for small h (for which the small localized state wave function approximation at the dielectric surface breaks down). The lower tunneling rate of the 3D model can be qualitatively understood as the result of the tunneling occurring via a finite cone of small angles θ, a fact not accounted for in the one-dimensional (1D) model. The analytical approximation also captures this difference with the 1D model, see Figs. 4(a) and 4(b).

Figures 4(a) and 4(b) show the relation between the tunneling rate W and the depth of the localized state, h, for a fixed tip-insulator distance d. The heights V_0 of spherical quantum well formed by a localized state are 4.5 and 7.6 eV, respectively, and all parameters are the same as those in Fig. 2, except the variable h. Note that the different slopes in Figs. 4(a) and 4(b) are due to the $1/r$ dependence of the localized state wave function which does not have a counterpart in the 1D solution. Figures 5(a) and 5(b) further illustrate the comparison between 3D and 1D models showing the tunneling rate dependence on the tip-sample separation d for a fixed value of the depth h.

We also perform a crude but reasonable comparison of our calculations with the experimental data, see Figs. 5(a) and 5(b). Such parameters as the barrier height, depth, and radius of the localized state are chosen to be as close to experimental conditions as possible. In Figs. 5(a) and 5(b), the heights V_0 of the spherical quantum well formed by localized states are 4.5 and 7.6 eV individually and all parameters are the same as those in Fig. 2 except the variable tip-sample distance d.

Since no tunneling can be observed if the tunneling rate is approximately less than one event per second, the tip-sample distance d should be between 0.8 and 1.3 nm. Indeed, as indicated by the data shown in Fig. 5(c), most tunneling events occur when the measured tip-sample distance falls within the interval of 0.7–1.3 nm, which is in a good agreement with the proposed model.

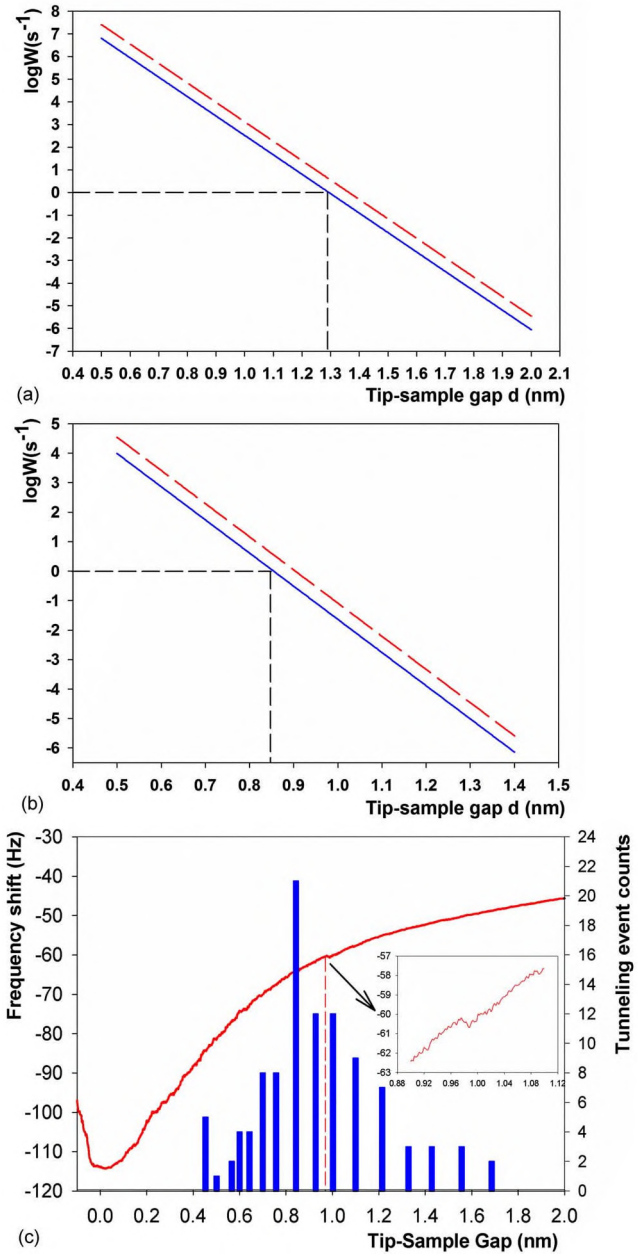

FIG. 5. (Color online) (a) Simulation curve of tunneling rate vs tip-sample gap and comparison of tunneling rate curves between the two models. The blue solid line is from the 3D analytical model, and the red dashed line is from the 1D model. All parameters in this simulation are the same as those in Fig. 2, except for V_0 and d. (b) Simulation curve of tunneling rate vs tip-sample gap and comparison of tunneling rate curve between the two models. The blue solid line is from the 3D analytical model, and red dashed line is from the 1D model. All parameters in this simulation are the same as those in Fig. 2, except for V_0 and d. (c) Typical curve of resonance frequency shift vs tip-sample gap measured near a sample with a 10 nm thick silicon dioxide film. A −4 V dc voltage is applied on the sample. The arrow indicates the position of a single-electron tunneling event and the tunneling event frequency shift is shown in the inset. The histogram shows the statistics of the measured tunneling events vs tip-sample gap. Most tunneling events occur when the tip-sample gap is between 0.7 and 1.3 nm.

The accuracy of this model is restricted by the use of Bardeen's approach as well as by the approximation in which the terms associated with the boundary condition at the dielectric surface are neglected. The neglecting of boundary condition terms is a more significant approximation, as it requires both wave functions to be small at the boundary, whereas Bardeen's approximation only requires that one of the wave functions be small at the boundary (weak coupling). More detailed calculations involving microscopic properties of the tip and the dielectric would improve the accuracy.

To summarize, we have presented a three-dimensional model for the calculation of tunneling rate between a conducting tip and a localized state in a dielectric surface as a function of several parameters characterizing the tip-surface geometry. The results are compared with similar calculations performed with the help of a one-dimensional model. The quantitative difference between the two models originates from the fact that the dominant contribution to tunneling comes from a finite range of electron states with wave vectors not exactly normal to the tip surface, $\theta \ll 1$. Experimental data are compared with the calculations, and a good agreement is reported.

ACKNOWLEDGMENTS

The authors acknowledge Y.-S. Wu and M. Raikh for helpful discussion. This work has been funded by the National Science Foundation DMR-0216711 and the Semiconductor Research Corporation.

[1] G. Binnig, H. Rohrer, Ch. Gerber, and E. Weibel, Phys. Rev. Lett. **49**, 57 (1982).
[2] L. J. Klein and C. C. Williams, Appl. Phys. Lett. **79**, 1828 (2001).
[3] L. J. Klein and C. C. Williams, Appl. Phys. Lett. **81**, 4589 (2002).
[4] E. Bussmann, D. J. Kim, and C. C. Williams, Appl. Phys. Lett. **85**, 2538 (2004).
[5] E. Bussmann, N. Zheng, and C. C. Williams, Appl. Phys. Lett. **86**, 163109 (2005).
[6] W. A. Harrison, *Applied Quantum Mechanics* (World Scientific, Singapore, 2000).
[7] J. Bardeen, Phys. Rev. Lett. **6**, 57 (1961).
[8] J. Tersoff, Phys. Rev. B **41**, 1235 (1990).
[9] C. J. Chen, *Introduction to Scanning Tunneling Microscopy* (Oxford University Press, New York, 1993).
[10] N. D. Lang, Phys. Rev. B **34**, 5947 (1986).
[11] D. A. Bonnell, *Scanning Tunneling Microscopy and Spectroscopy: Theory, Techniques, and Applications* (John Wiley & Sons, New York, 1993).